CHAPTER TWELVE

Time-Resolved X-ray Scattering and RNA Folding

Lois Pollack* *and* Sebastian Doniach[†,‡]

Contents

Abstract

Time-resolved small-angle X-ray scattering (SAXS) reports changes in the global conformation of macromolecules and is thus a valuable probe of structural transitions like RNA folding. Time-resolved SAXS has been applied to study folding of the *Tetrahymena* ribozyme. This chapter describes the methods that enable acquisition and analysis of time-resolved SAXS data and insights into RNA folding gained from these studies.

* School of Applied and Engineering Physics, Cornell University, Ithaca, New York, USA
† Department of Applied Physics, Stanford University, Stanford, California, USA
‡ Department of Physics, Stanford University, Stanford, California, USA

Methods in Enzymology, Volume 469
ISSN 0076-6879, DOI: 10.1016/S0076-6879(09)69012-1

1. Introduction

Conformational changes in biomolecules, including folding, can be induced by solvent exchange through mixing. For proteins, this change is usually accomplished by diluting a solution of a protein–denaturant mixture (urea or guanidine hydrochloride) with buffer so that the resulting solvent has a denaturant concentration well below a threshold for denaturation. For polynucleotides such as RNA, denaturation results from the repulsive Coulomb forces between phosphate groups in the phosphate–sugar backbone which are imperfectly screened in a buffer containing minimal monovalent salt (NaCl or KCl). In these systems folding is induced by the addition of buffer containing higher concentrations of cations, typically 10 m*M* Mg^{2+} (as $MgCl_2$).

Small-angle X-ray scattering (SAXS) provides valuable information about the global structure of macromolecules, such as the size and shape of RNA (Lipfert and Doniach, 2007). Time-resolved SAXS reports the changes in the global conformation that accompany a structural transition like folding.

The earliest time-resolved SAXS studies of RNA folding (Russell *et al.*, 2000) relied on manual mixing techniques and reported significant compaction of unfolded RNA within 30 s of the addition of Mg^{2+}. Access to shorter measurement times was enabled by application of rapid mixing devices. Stopped flow mixers were used to measure folding events on time scales as short as tens of milliseconds after initiation of folding (Russell *et al.*, 2002); more specialized continuous flow mixers accessed times beginning within about 1 ms of the initiation of folding (Akiyama *et al.*, 2002; Pollack *et al.*, 1999). Application of these techniques to the RNA folding problem has revealed discrete and temporally well-resolved phases of molecular compaction triggered by the addition of cations (Das *et al.*, 2003; Russell *et al.*, 2002). These transitions occur on time scales as short as single millisecond and as long as minutes. In conjunction with studies of mutants (Das *et al.*, 2003; Kwok *et al.*, 2006) or when coupled with other techniques that report local structure formation on comparable time scales (Kwok *et al.*, 2006; Schlatterer *et al.*, 2008), time-resolved SAXS experiments have helped to provide insight into the mechanisms that drive large-scale conformational transitions. This chapter describes the methods involved in acquiring and interpreting time-resolved SAXS data of RNA folding.

2. SAXS Studies of RNA

We begin with a brief review of static SAXS (see Chapter 11 of this volume). X-rays incident on a sample are deflected or scattered by objects with electron densities that differ from that of the surrounding buffer. For

objects with dimensions larger than the X-ray wavelength, typically 1 Å, the angular dependence of the scattering intensity reflects phase differences between X-rays scattered from electrons at different positions within the object. The intensity falls off more rapidly with angle for a larger (compared to smaller) object, as more substantial phase differences result from the larger distances present.

Because SAXS reports molecular conformation in solution, it is ideally suited to measure conformational changes, for example, those due to folding; however, the molecules in solution are randomly oriented with respect to the beam, thus the spatially averaged structure is measured. This latter consideration is important in interpreting SAXS data.

3. Data Acquisition

Small-angle scattering profiles report the intensity of X-rays scattered as a function of angle, relative to the $\theta = 0°$ direction of the incident beam. Typically, intensity is plotted as a function of $q = 4\pi \sin \theta/\lambda$ or $s = 2 \sin \theta/\lambda = q/2\pi$. A cartoon representing a SAXS beamline is shown in Fig. 12.1. Two profiles must be acquired to extract the scattering originating from the macromolecule. The first measures the scattering of RNA plus buffer in the cell. This signal also includes parasitic photons. The second measures scattering from buffer alone in the cell along with the parasitic signal. All profiles are scaled to compensate for variations in X-ray beam intensity, monitored by a diode that is integrated into the beam stop (see Fig. 12.1) and by ionization chambers placed before the sample. The "RNA absent" or background profile is subtracted from the "RNA

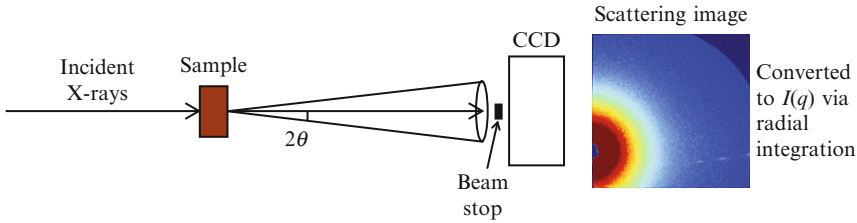

Figure 12.1 A schematic representation of a SAXS experiment. The X-ray beam is incident from the left and scatters from the sample. A detector, located to the right of the sample, records the angular variation of intensity of scattered X-rays. The shape of this scattering profile contains information about the global structural features of the molecules in the sample. More details about the beamline components, as well as the process for converting CCD images into one dimensional curves of intensity versus angle, can be found elsewhere in this volume (Chapter 19).

present'' profile, yielding the scattering profile of the RNA alone. Note that the background signal contains contributions not only from the buffer but also from all windows and other components along the beamline, including notorious slit scatter that should be minimized but cannot always be eliminated. It is important to note that this so-called ''parasitic scattering'' tends to be greatest in the forward direction, surrounding the beam stop.

Standard experimental protocol suggests that ''background'' images be acquired both before and after an RNA-containing image, using the same sample cell whenever possible. The ''before'' and ''after'' scattering profiles should match identically and can then be subtracted from the RNA scattering profile.

Signal averaging is almost always required for time-resolved measurements. Signals are small because of the relatively low number of scattered photons resulting from the short exposure times employed for manual mixing or stopped flow measurements or the small sample volumes associated with continuous flow mixers.

4. Time-Resolved SAXS Methods

Time-resolved SAXS studies report the time course of conformational changes following the addition of cations that trigger RNA folding. The ultimate time resolution of these experimental methods is determined both by the type of mixer used and the measurement time.

4.1. Stopped flow mixers and RNA folding

Mixing times of several milliseconds are typical for stopped flow, though newer commercial mixers boast dead times approaching the single millisecond. After mixing, solutions are ejected into a SAXS compatible cell, described in more detail in Section 4.1.1. The X-ray beam may be gated to collect snapshots of the scattering profile at a predetermined set of intervals in order to minimize the total radiation exposure and hence the radiation damage to the sample. Short exposures are acquired after mixing is complete, at carefully calibrated delay times. In this case the time resolution is determined by the shortest opening time of the shutter and by the sensitivity of the detector. Alternatively, the sample can be exposed continuously to the X-ray beam and the detector read periodically. As the readout time of typical CCD detectors may be quite slow (hundreds of milliseconds), this also limits the time resolution of the measurement. Again, total radiation dose needs to be minimized to avoid excessive radiation damage to the sample. In these experiments, timing is controlled by computer coordination between the mixer and the beamline shutter or detector. Stopped

flow places no restrictions on the longest time delays, in principle the sample can be left to age for hours; however, repeated exposure of the same sample should be avoided as it can result in radiation damage.

4.1.1. Stopped flow instrumentation

Commercially available stopped flow mixers (from BioLogic as used at the Advanced Photon Source (APS) and the Cornell High Energy Synchrotron Source (CHESS) or Unisoku, Osaka, Japan, as used at Stanford Synchrotron Radiation Laboratory (SSRL)) can be readily modified for compatibility with synchrotron X-ray beams. The mixed sample is pushed either into customized cuvettes, machined to fit into the mixer head, or into X-ray compatible capillaries. The path length of the cuvettes/capillary can be adjusted for any X-ray energy; for example, a 1-mm path length works well at X-ray energies of 8 keV. Most importantly, the ''windows'' on the cuvette, through which X-rays pass, must not contribute significantly to the overall background scattering. Both mica and silicon nitride windows have been successfully employed for SAXS experiments (Andresen *et al.*, 2004; Lipfert *et al.*, 2006).

4.2. Continuous flow mixers and RNA folding

Continuous flow mixers are employed to access folding events on timescales shorter than 10 ms. In addition to sharp time resolution, the use of continuous flow remediates radiation damage because the (constantly replenished) sample is only briefly exposed to the X-ray beam. As indicated above, the mixing time of RNA with Mg^{2+} is a critical factor in determining the time resolution of the experiment. Mixing times as short as tens of microseconds have been demonstrated using microfluidic mixers with hydrodynamic focusing (Park *et al.*, 2006), although the mixing time of the present generation of SAXS compatible mixers (shown schematically in Fig. 12.2) is of order 1 ms. RNA is unfolded in a low salt buffer and flows into one port of the continuous flow mixer. An equivalent buffer containing an additional 10 m*M* $MgCl_2$ flows into two orthogonal ports. The flow of these two channels focuses the RNA-containing solution into a thin jet. Diffusion of small Mg^{2+} ions across this stream occurs rapidly, triggering folding. The RNA folds as it flows down the channel; the device can be translated relative to the X-ray beam to probe the RNA conformation at any position. In this way measurement of time delay is converted into distance of the point of measurement from the point of mixing, divided by the velocity of the stream. Hence, time dependence is measured within this mixer by sampling numerous positions along the outlet channel. In the simplest case, the ''time resolution'' of the measurement is determined by the passage time of flowing sample across the beam-defined window. For

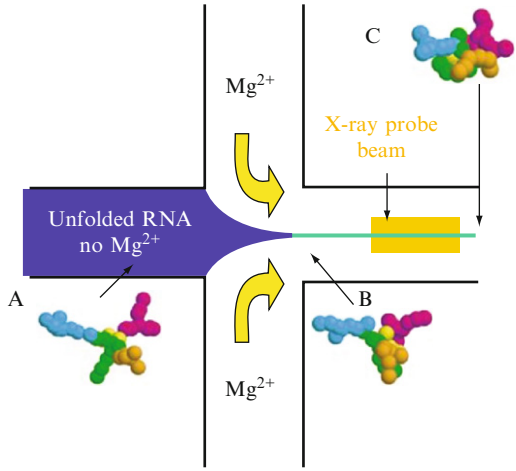

Figure 12.2 A schematic of continuous flow mixers used for time-resolved SAXS studies of RNA folding. The molecular shapes depicted in the figure represent coarse grain models of RNA conformations, described in Russell *et al.* (2002).

example, if the stream flows at 10 cm/s and the X-ray beam width is 10 μm, the time resolution of the measurement equals 100 μs.

The time resolution of the measurement also depends on several important mixer parameters: the diffusive mixing time (determined by the jet width and the diffusion coefficient of the ions (Knight *et al.*, 1998)), the beam size, uncertainty in the mixing time resulting from the hydrodynamic focusing process, and depth-dependent variations in the flow speed of the jet. Each of these issues has been addressed independently, but will be briefly reviewed here for completeness.

The first uncertainty arises from premature mixing of RNA with Mg^{2+} ions as the jet is being focused. The RNA that flows along the edges of the jet contacts Mg^{2+} at an earlier time than the RNA that flows along the midplane of the device. Premixing times depend both on channel dimension and flow speed, and introduce uncertainty on the order of 1 ms into the mixing times. These effects can be eliminated using a more complicated mixer, employing sheath flow (Park *et al.*, 2006).

Time resolution can also be limited by the parabolic flow profile of a confined fluid in the low Reynolds number (laminar flow) regime. The fluid velocity at the walls approaches zero. If the probe beam sample molecules spread over the entire width of a channel, their differing velocities must be considered. Those in close proximity to the walls travel very slowly, whereas those at the center of the channel flow most rapidly. To compensate for this effect, we flow an extra layer of buffer against the walls

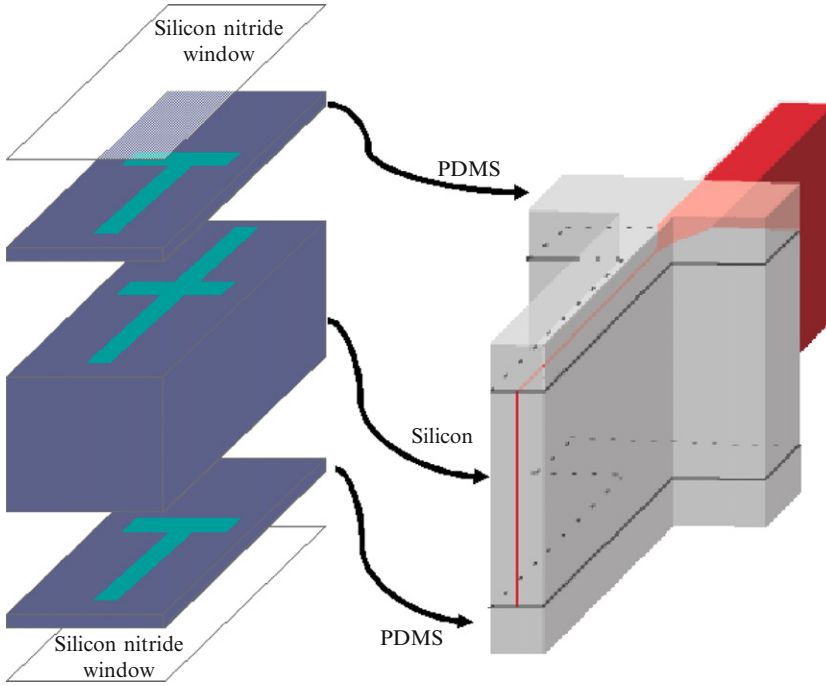

Figure 12.3 A more realistic depiction of the hydrodynamic focusing mixer used for time-resolved SAXS studies. This figure, adapted from Lisa Kwok's thesis (Ph.D. Cornell), illustrates the multilayer construction of the mixing device.

where the velocity gradient is largest. Figure 12.3 illustrates a more realistic schematic of the mixer. Its fabrication is described in Section 5. An additional benefit of this more complex geometry is the lack of contact between RNA and the windows, which eliminates concerns about sample sticking.

5. Mixer Fabrication

The rapid mixer is composed of layers that are fabricated separately and then assembled together. The main four channel device, represented by the cartoon of Fig. 12.2, is etched through a 1-mm-thick silicon wafer using an anisotropic Bosch process RIE (Unaxis 770, Unaxis). The depth of this etch requires a thick mask. We use a 7 μm layer of PECVD silicon dioxide (GCI PECVD; Group Sciences Incorporated, San Jose, CA). This mixer is sandwiched between two 100 μm thick poly(dimethylsiloxane) (PDMS) layers (Duffy *et al.*, 1998), which contain channels in a T configuration.

These three channels overlay the side and outlet channels of the mixer and provide the buffer flow that separates the RNA-containing jet from the windows. These layers were fabricated by curing PDMS onto masters created by selectively exposing SU-8 photoresist. Finally, the PDMS–silicon device is sandwiched between two silicon nitride windows. These windows are fabricated by coating a wafer with a thin silicon nitride film, then through etching from the bottom to expose rectangular silicon nitride membranes. The silicon is cut to size, and these windows are attached to the PDMS layers, forming a complete device. Additional liquid PDMS is used to seal the device, if necessary.

Once assembled, the device is mounted in a stainless steel holder. A large ($\sim$mm^2) pad, fabricated at the end of each channel, serves as the interface between external plumbing and the microfluidic channels. The custom-machined holder contains a series of channels that interface on one end with the fabricated pad and on the other end with standard connectors for Luer lock tubing. O-rings positioned between the stainless steel holder and the chip reservoirs provide the required fluid seal. The Luer lock fittings interface the chips to standard tubing and eventually to syringes that contain the samples and buffers. Finally, Harvard syringe pumps are used to drive the flow through the channels. Precision syringe pumps (Harvard PHD 2000 Harvard Apparatus) are used to drive the RNA-containing solution, while more robust pumps (Harvard 22) are used to drive the substantial buffer flow. By varying the settings on the pumps, flow speeds ranging from mm/s through tens of cm/s can be achieved. Both short and long times can be easily accessed in a single device. These mixers enable studies on time scales ranging from submillisecond up to 0.2 s.

5.1. X-ray beam parameters

Because of the short measurement times of stopped flow, or the small sample volumes associated with continuous flow, a synchrotron source is required for time-resolved SAXS studies of RNA folding. To date studies have been carried out at the APS, at CHESS, and at SSRL. The optics vary by beamline, but all involve intensity enhancement by an insertion device. Monochromatic undulator beam was employed for stopped flow experiments at the 12-ID station at APS (Seifert *et al.*, 2000). Multilayer beam was employed at SSRL beamline 4-2 (Tsuruta *et al.*, 1998), and focused multilayer beam was employed at the CHESS G1 station (Kazimirov *et al.*, 2006). For the continuous flow cell, ''pink'' or 3% bandwidth undulator beam was employed at the 8-ID beamline at APS (Sandy *et al.*, 1999). All experiments employed a CCD detector to record a 2D image of the scattering, as illustrated in Fig. 12.1.

5.2. Sample preparation

Since RNA secondary structure is relatively stable, RNA folding experiments which start with a sample that has been prepared in the absence of Mg^{2+} generally need to anneal the sample in a suitable buffer at relatively high temperatures between 50 and 90 °C.

This observation is a result of experiments on folding of the *Tetrahymena* ribozyme, in which a kinetically stable misfolded state was found to form when folding was initiated by addition of Mg^{2+} for a sample prepared at low temperature (Russell *et al.*, 2002). This state was shown to give an R_g value of 51 Å, identical to that for the folding intermediate. A subsequent 50 °C incubation was required to achieve the reduced R_g of the native state. It is important to note that the pathways that lead to the native and misfolded states diverge from each other late in folding, concomitant with or subsequent to the rate-limiting step. This indicates that the 51 Å intermediate that was observed prior to the rate-limiting step is populated by molecules that fold correctly as well as incorrectly.

This kind of observation has led to the idea that functional RNA molecules tend to fold an order of magnitude more slowly than proteins, as kinetic traps may form on the folding pathway which then take time to unfold again so that the molecule can finally reach its functional folded state. However, the lack of time-resolved RNA folding measurements to date on a range of different functional RNAs means that this idea has not yet been substantiated in depth.

5.3. Samples and radiation damage

Acquisition of a complete time series typically requires between 1 and 10 mg of RNA, dissolved to concentrations between 1 and 4 mg/ml. As a control for aggregation due to the relative high RNA concentration, data are acquired at two or three different concentrations. Ample quantities of RNA were prepared by *in vitro* transcription and purified as described in Russell and Herschlag (1999) and Schlatterer *et al.* (2008). Molecules were unfolded in 50 m*M* Na-MOPS or K-MOPS buffer, pH 7.0. In most cases folding was initiated by the addition of buffer containing sufficient $MgCl_2$ to raise the free concentration of Mg^{2+} to 10 m*M*.

The high flux of synchrotron X-rays generates large numbers of hydroxyl radicals that can radiation damage RNA samples (e.g., Sclavi *et al.*, 1997). Radiation damage is manifested by time-dependent changes in scattering profiles, most notably at the lowest angle, which signify aggregation. These changes can be small, but accumulate with time. As mentioned above, flow cells remediate this damage, but increase the rate of RNA consumption. Further measures that limit radiation damage include the use of Tris–HCl buffer that rapidly scavenged hydroxyl radicals (Fang *et al.*, 2000).

6. Data Analysis of SAXS Measurements

6.1. Radius of gyration

Early time-resolved data on protein folding emphasized the time dependence of the forward scattering intensity $I(0)$ and the radius of gyration R_g (Chen *et al.*, 1996, 1998; Eliezer *et al.*, 1993, 1995). Radius of gyration values were calculated using the Guinier approximation. The first time-resolved SAXS studies of *Tetrahymena* ribozyme folding (Russell *et al.*, 2000) were achieved by manual mixing. Russell *et al.* reported changes in the radius of gyration of this ribozyme upon initiation of tertiary folding by the addition of Mg^{2+} to RNA under low-salt conditions. The R_g value decreased from 74 to 51 Å within the experimental dead time of 1 min, yielding a minimum rate constant for the compaction of 3 min^{-1}, at least 20-fold faster than the overall rate constant for folding. Under these experimental conditions (15 °C), 95% of the ribozyme population misfolds to a state that is stable for hours, but rapidly converts to the native state, with an R_g of 47 Å at elevated temperature (Russell and Herschlag, 1999). These experiments indicate that a compact set of intermediates forms early in the folding process.

Despite the straightforward nature of these measurements, it took several years before the radius of gyration of a full folding course could be measured, largely due to experimental difficulties in accessing very low angle data due to parasitic scattering. Kwok *et al.* (2006) reported time-dependent R_g measured over the full course of folding. Representative curves are shown in Fig. 12.4 for the wild-type ribozyme initiated from a standard (20 m*M*) low-salt initial condition as well as from a higher salt (100 m*M*) initial condition. Both continuous and stopped flow techniques were employed. Time-resolved SAXS studies of the full-length ribozyme display a number of discrete transitions, with amplitudes that depend on the presence of specific tertiary contacts as well as on salt conditions. The parallel application of a local structural probe, in this case time-dependent hydroxyl radical footprinting, was essential in interpreting the R_g data. Application of these coupled techniques clearly indicated that a rapid compaction occurs prior to significant tertiary contact formation in the full-length ribozyme (Kwok *et al.*, 2006). Comparable studies on folding of the P4–P6 domain display compaction that is more coincident with tertiary contact formation and suggest that folding of this domain is limited by stiff hinges in addition to electrostatics (Schlatterer *et al.*, 2008).

6.2. Principal component analysis

Although the radius of gyration provides the overall size of the molecule, the full scattering profile contains much additional information. Segel *et al.* (1999) introduced the use of principal component analysis of the kinetics (see also Doniach, 2001) to separate scattering profiles of intermediate states

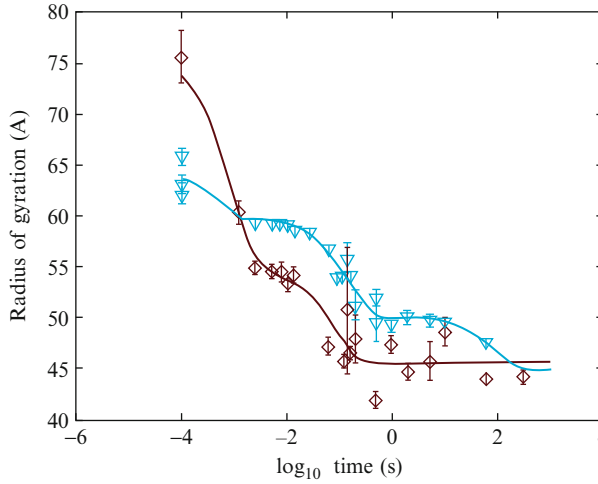

Figure 12.4 The time-dependent radius of gyration for the *Tetrahymena* ribozyme following the addition of 10 m*M* Mg^{2+} to RNA in solutions containing either low (20 m*M*, brown) or moderate (100 m*M*, blue) concentrations of monovalent ions.

occupied along the kinetic folding pathway. This approach was successfully applied in the first full time-resolved studies of RNA folding, combining both continuous and stopped flow data (Russell *et al.*, 2002). Here, data acquired for folding times ranging from 5 ms to 1000 s were fit according to singular value decomposition (SVD) analysis (Doniach, 2001; Henry and Hofrichter, 1992). This analysis identifies the smallest number of independent curves that, in different combination, can recreate a dataset of related experimental curves. A matrix representing the experimental data is created with columns corresponding to scattering profiles acquired at different times. SVD (MATLAB) is used to transform this matrix of scattering profiles in a product of three matrices: $[U\ W\ V]^{T}$. The leftmost matrix, U, contains the set of column vectors that form an orthonormal basis for the data matrix. The center matrix, W, is diagonal and contains the so-called singular values for each basis curve in U. These coefficients dictate the weight of each basis curve that is needed to accurately reconstruct each experimental curve. Finally, V provides a measure of the weights of each basis curve required to reconstruct the data. V contains the amplitudes of each basis vector for the initial data profiles being analyzed. The number of significant singular values (i.e., with a magnitude significantly larger than noise) indicates the number of independent basis curves required to completely reconstruct the data.

Application of SVD analysis to the time-resolved SAXS data of Russell *et al.* (2002) clearly indicated two significant singular values, and therefore enabled data analysis by projection of each independent scattering profile onto two states. The folded and unfolded states were selected because of

their physical significance. A least-squares fit was used to optimize this decomposition. In most cases, analysis of the residuals of the fit was consistent with random noise, confirming the applicability of this method. In some cases small systematic deviation was observed, suggesting the need for a third SVD component; however, inclusion of an additional component did not significantly alter the conclusions of the analysis based on two components.

This decomposition was applied to curves displaying the product of Is^2 versus s; plots of SAXS data in this form are called Kratky plots. This format readily distinguished extended from compact conformations and emphasizes changes in scattering profiles at larger angle, reflecting subtle yet significant changes in molecular conformation. Kratky plots of unfolded RNA typically have a small shoulder or peak at low angle, followed by a gentle rise. Folded RNA, which are much more compact, display strong peaks in the low to mid angle region.

This analysis was applied in the first millisecond scale studies of RNA folding (Russell *et al.*, 2002) in addition to follow-up studies (Das *et al.*, 2003) that probed folding of a mutant RNA in which the five long range tertiary contacts were knocked out. Figure 12.5 shows Kratky plots in addition to the coefficients of the linear projection of each time-dependent scattering profile on the unfolded and folded states. Each set of fractional weights can be fit to a double (for the wild-type) or single (for the knockout mutant) exponential to extract kinetic parameters. The data shown in this figure were acquired via both continuous (open circles) and stopped (closed circles) flow. For all datasets, SVD analysis reveals two dominant components. However, the presence of more than two states cannot be ruled out (Das *et al.*, 2003).

6.3. Three-dimensional reconstruction from one-dimensional SAXS data

Analysis of the data in terms of low-resolution three-dimensional electron density maps of the scattering molecules in different states dates back to Svergun and Stuhrmann (1991). This approach received a qualitative advance by the work of Chacon *et al.* (1998), who showed how density maps could be generated by placing point scatters on a grid to reproduce the observed scattering profile. The key step here is the breaking of isotropic symmetry of the data by placing scattering centers (“beads”) on a lattice. The uniqueness of the resulting reconstructions was investigated for several proteins by Walther *et al.* (2000), who also developed an algorithm (SAXS 3d) for generating the bead models. At the same time, Svergun and collaborators (Petoukhov and Svergun, 2003; Svergun, 1999) developed algorithms DAMMIN and GASBOR for building bead models which are now widely used.

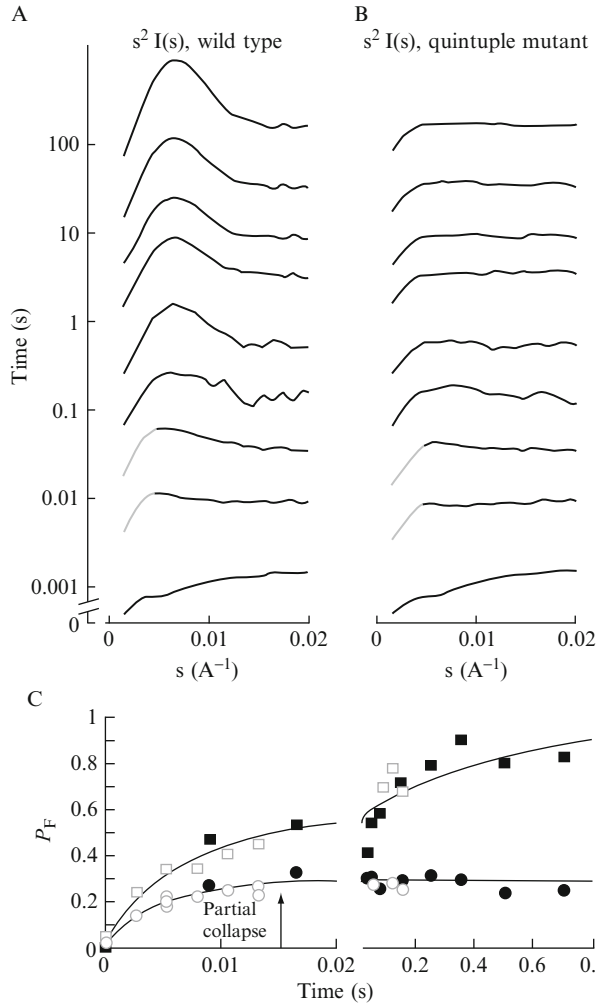

Figure 12.5 SAXS data representing a full time series following the addition of Mg^{2+} to trigger folding of the *Tetrahymena* ribozyme. Scattering profiles of two constructs are shown as Kratky plots. Panel (A) illustrates folding of the wild-type ribozyme. Panel (B) illustrates folding of a construct in which five key long range contacts have been disrupted by mutation. Panel (C) illustrates the two-state projections described in the text. Here, P_F represents the percentage of the "folded" scattering profile that provides the best fit to each time-dependent curve. Data are shown for both the wild-type (squares) and mutant (circle) ribozymes (Figure reprinted with permission from Das *et al.*, 2003).

Application of these algorithms to SAXS data on small RNA molecules was initiated by Lipfert and Doniach (2007), who showed that three-dimensional density maps giving the shape outline of small RNAs and

DNAs (such as tRNA and short DNA duplexes) generated from SAXS data fitted the X-ray crystallography—derived structures at low resolution on the scale of 10–15 Å.

In a recent study, Pollack and collaborators (Lamb *et al.*, 2008) applied shape generation algorithms to RNA folding measurements. They investigated the limits of applicability of reconstruction methods to time-resolved data by providing examples and discussing the pros and cons of this approach, in particular addressing two primary concerns. First, signal-to-noise ratio associated with time-resolved data is much lower than that of equilibrium data. Time-resolved data are more subject to noise from parasitic scattering that can only be subtracted out in an average way than are static data for which longer exposure times allow better averaging over fluctuations in the parasitic scattering. Each individual time-resolved measurement will thus have a variable parasitic background making the analysis of multiple components contributing to the overall scattering profile more difficult. Thus, more detailed study of time-resolved intermediates in RNA conformation changes will require averaging over many time-resolved scattering runs. Second, during folding, the ensemble of states present may be more heterogeneous than in a static experiment, especially if multiple parallel pathways are present. In an attempt to reconstruct a reaction intermediate, this approach was only applied to ''long lived'' intermediates, for example, those states occurring during a plateau in the kinetic curve.

7. Concluding Remarks

SAXS data have the advantage of providing information of global changes in molecular conformation. In this sense it is complementary to local probes of RNA structure such as NMR, FRET, fluorescent probes, single-molecule measurements, and hydroxyl radical footprinting. It also has the advantage of time resolution over time scales ranging from tens of microseconds to hours. The disadvantages are the fairly large quantities of sample needed to overcome radiation damage limitations and the need to use specialized synchrotron radiation facilities.

ACKNOWLEDGMENTS

We acknowledge our collaborators for help and discussions, in particular: K. Andresen, Y. Bai, M. Brenowitz, R. Das, S. M. Gruner, D. Herschlag, J. Jacob, L. W. Kwok, J. S. Lamb, G .S. Maskel, T. T. Mills, I. S. Millett, S. G. J. Mochrie, B. Nakatani, V. Pande, H. Y. Park, R. Russell, J. Schlatterer, S. Seifert, I. Shcherbakova, H. Smith, M. W. Tate and P. Thiyagarajan.

This research was generously supported by NIH grant PO1 GM066275, NASA through (NAG8-1178) and NSF through Cornell's Nanobiotechnology Center and through MCB-0347220. Computing resources were provided by the Bio-X2 computer cluster at Stanford University (NSF award CNS-0619926). Use of the Advanced Photon Source was supported by the U.S. Department of Energy, Office of Science, and Office of Basic Energy Sciences, under Contract No. DE-AC02-06CH11357. CHESS is supported by the NSF and the NIH/National Institute of General Medical Sciences under award DMR-0225180.

REFERENCES

Akiyama, S., Takahashi, S., Kimura, T., Ishimori, K., Morishima, I., Nishikawa, Y., and Fujisawa, T. (2002). Conformational landscape of cytochrome c folding studied by microsecond-resolved small-angle X-ray scattering. *Proc. Natl. Acad. Sci. USA* **99,** 1329–1334.

Andresen, K., Das, R., Park, H. Y., Smith, H., Kwok, L. W., Lamb, J. S., Kirkland, E. J., Herschlag, D., Finkelstein, K. D., and Pollack, L. (2004). Spatial distribution of competing ions around DNA in solution. *Phys. Rev. Lett.* **93,** 248103.

Chacon, P., Moran, F., Diaz, J. F., Pantos, E., and Andreu, J. M. (1998). Low-resolution structures of proteins in solution retrieved from X-ray scattering with a genetic algorithm. *Biophys. J.* **74,** 2760–2775.

Chen, L. L., Hodgson, K. O., and Doniach, S. (1996). A lysozyme folding intermediate revealed by solution X-ray scattering. *J. Mol. Biol.* **261,** 658–671.

Chen, L. L., Wildegger, G., Kiefhaber, T., Hodgson, K. O., and Doniach, S. (1998). Kinetics of lysozyme refolding: Structural characterization of a non-specifically collapsed state using time-resolved X-ray scattering. *J. Mol. Biol.* **276,** 225–237.

Das, R., Kwok, L. W., Millett, I. S., Bai, Y., Mills, T. T., Jacob, J., Maskel, G. S., Seifert, S., Mochrie, S. G. J., Thiyagarajan, P., Doniach, S., Pollack, L., *et al.* (2003). The fastest global events in RNA folding: Electrostatic relaxation and tertiary collapse of the *Tetrahymena* ribozyme. *J. Mol. Biol.* **332,** 311–319.

Doniach, S. (2001). Changes in biomolecular conformation seen by small angle X-ray scattering. *Chem. Rev.* **101,** 1763–1778.

Duffy, D. C., McDonald, J. C., Schueller, O. J. A., and Whitesides, G. M. (1998). Rapid prototyping of microfluidic systems in poly(dimethylsiloxane). *Anal. Chem.* **70,** 4974–4984.

Eliezer, D., Chiba, K., Tsuruta, H., Doniach, S., Hodgson, K. O., and Kihara, H. (1993). Evidence of an associative intermediate on the myoglobin refolding pathway. *Biophys. J.* **65,** 912–917.

Eliezer, D., Jennings, P. A., Wright, P. E., Doniach, S., Hodgson, K. O., and Tsuruta, H. (1995). The radius of gyration of an apomyoglobin folding intermediate. *Science* **270,** 487–488.

Fang, X. W., Littrell, K., Yang, X., Henderson, S. J., Siefert, S., Thiyagarajan, P., Pan, T., and Sosnick, T. R. (2000). Mg^{2+}-dependent compaction and folding of yeast tRNA (Phe) and the catalytic domain of the B-subtilis RNase P RNA determined by small-angle X-ray scattering. *Biochemistry* **39,** 11107–11113.

Henry, E. R., and Hofrichter, J. (1992). Singular value decomposition—Application to analysis of experimental-data. *Methods Enzymol.* **210,** 129–192.

Kazimirov, A., Smilgies, D. M., Shen, Q., Xiao, X. H., Hao, Q., Fontes, E., Bilderback, D. H., Gruner, S. M., Platonov, Y., and Martynov, V. V. (2006). Multilayer X-ray optics at CHESS. *J. Synchrotron Radiat.* **13,** 204–210.

Knight, J. B., Vishwanath, A., Brody, J. P., and Austin, R. H. (1998). Hydrodynamic focusing on a silicon chip: Mixing nanoliters in microseconds. *Phys. Rev. Lett.* **80,** 3863–3866.

Kwok, L. W., Shcherbakova, I., Lamb, J. S., Park, H. Y., Andresen, K., Smith, H., Brenowitz, M., and Pollack, L. (2006). Concordant exploration of the kinetics of RNA folding from global and local perspectives. *J. Mol. Biol.* **355,** 282–293.

Lamb, J., Kwok, L., Qiu, X. Y., Andresen, K., Park, H. Y., and Pollack, L. (2008). Reconstructing three-dimensional shape envelopes from time-resolved small-angle X-ray scattering data. *J. Appl. Crystallogr.* **41,** 1046–1052.

Lipfert, J., and Doniach, S. (2007). Small-angle X-ray scattering from RNA, proteins, and protein complexes. *Annu. Rev. Biophys. Biomol. Struct.* **36,** 307–327.

Lipfert, J., Millett, I. S., Seifert, S., and Doniach, S. (2006). Sample holder for small-angle X-ray scattering static and flow cell measurements. *Rev. Sci. Instrum.* **77**, 046108.

Park, H. Y., Qiu, X. Y., Rhoades, E., Korlach, J., Kwok, L. W., Zipfel, W. R., Webb, W. W., and Pollack, L. (2006). Achieving uniform mixing in a microfluidic device: Hydrodynamic focusing prior to mixing. *Anal. Chem.* **78,** 4465–4473.

Petoukhov, M. V., and Svergun, D. I. (2003). New methods for domain structure determination of proteins from solution scattering data. *J. Appl. Crystallogr.* **36,** 540–544.

Pollack, L., Tate, M. W., Darnton, N. C., Knight, J. B., Gruner, S. M., Eaton, W. A., and Austin, R. H. (1999). Compactness of the denatured state of a fast-folding protein measured by submillisecond small-angle X-ray scattering. *Proc. Natl. Acad. Sci. USA* **96,** 10115–10117.

Russell, R., and Herschlag, D. (1999). New pathways in folding of the *Tetrahymena* group I RNA enzyme. *J. Mol. Biol.* **291,** 1155–1167.

Russell, R., Millett, I. S., Doniach, S., and Herschlag, D. (2000). Small angle X-ray scattering reveals a compact intermediate in RNA folding. *Nat. Struct. Biol.* **7,** 367–370.

Russell, R., Millettt, I. S., Tate, M. W., Kwok, L. W., Nakatani, B., Gruner, S. M., Mochrie, S. G. J., Pande, V., Doniach, S., Herschlag, D., and Pollack, L. (2002). Rapid compaction during RNA folding. *Proc. Natl. Acad. Sci. USA* **99,** 4266–4271.

Sandy, A. R., Lurio, L. B., Mochrie, S. G. J., Malik, A., Stephenson, G. B., Pelletier, J. F., and Sutton, M. (1999). Design and characterization of an undulator beamline optimized for small-angle coherent X-ray scattering at the advanced photon source. *J. Synchrotron Radiat.* **6,** 1174–1184.

Schlatterer, J. C., Kwok, L. W., Lamb, J. S., Park, H. Y., Andresen, K., Brenowitz, M., and Pollack, L. (2008). Hinge bending: A barrier to RNA folding. *J. Mol. Biol.* **379,** 859–870.

Sclavi, B., Woodson, S., Sullivan, M., Chance, M. R., and Brenowitz, M. (1997). Time-resolved synchrotron X-ray ''footprinting'', a new approach to the study of nucleic acid structure and function: Application to protein-DNA interactions and RNA folding. *J. Mol. Biol.* **266,** 144–159.

Segel, D. J., Bachmann, A., Hofrichter, J., Hodgson, K. O., Doniach, S., and Kiefhaber, T. (1999). Characterization of transient intermediates in lysozyme folding with time-resolved small-angle X-ray scattering. *J. Mol. Biol.* **288,** 489–499.

Seifert, S., Winans, R. E., Tiede, D. M., and Thiyagarajan, P. (2000). Design and performance of a ASAXS instrument at the advanced photon source. *J. Appl. Crystallogr.* **33,** 782–784.

Svergun, D. I. (1999). Restoring low resolution structure of biological macromolecules from solution scattering using simulated annealing. *Biophys. J.* **76,** 2879–2886.

Svergun, D. I., and Stuhrmann, H. B. (1991). New developments in direct shape determination from small-angle scattering. I. Theory and model-calculations. *Acta Crystallogr. A* **47,** 736–744.

Tsuruta, H., Brennan, S., Rek, Z. U., Irving, T. C., Tompkins, W. H., and Hodgson, K. O. (1998). A wide-bandpass multilayer monochromator for biological small-angle scattering and fiber diffraction studies. *J. Appl. Crystallogr.* **31,** 672–682.

Walther, D., Cohen, F. E., and Doniach, S. (2000). Reconstruction of low-resolution three-dimensional density maps from one-dimensional small-angle X-ray solution scattering data for biomolecules. *J. Appl. Crystallogr.* **33,** 350–363.